One-step green preparation of magnetic seaweed biochar/sulfidated Fe^0 composite with strengthen adsorptive removal of tetrabromobisphenol A through in situ reduction

Cui Zhang[a,b], Jian Lu[a,b,c,*], Jun Wu[d]

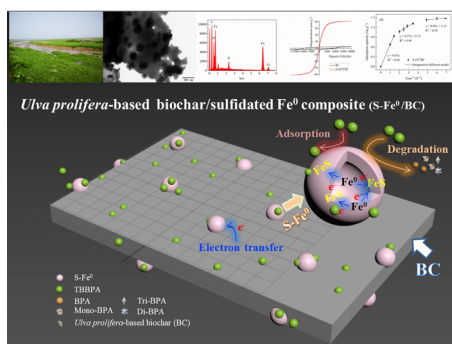[a] CAS Key Laboratory of Coastal Environmental Processes and Ecological Remediation, Yantai Institute of Coastal Zone Research (YIC), Chinese Academy of Sciences (CAS), Shandong Key Laboratory of Coastal Environmental Processes, YICCAS, Yantai, Shandong 264003, PR China
[b] University of Chinese Academy of Sciences, Beijing, 100049, PR China
[c] Center for Ocean Mega-Science, Chinese Academy of Sciences, 7 Nanhai Road, Qingdao, Shandong 266071, PR China
[d] School of Resources and Environmental Engineering, Ludong University, Yantai, Shandong 264025, PR China

GRAPHICAL ABSTRACT

ARTICLE INFO

ABSTRACT

Rare information is available on the facile preparation of biochar/sulfidated Fe^0 composite. A facile one-step green method was established for the synthesis of magnetic seaweed (*Ulva prolifera*) biochar/sulfidated Fe^0 composite (S-Fe^0/BC) to use excessive seaweed biomass. Removal efficiency of tetrabromobisphenol A (TBBPA) reached up to 88% in iron-sulfur treatment. Two major products were identified as bisphenol A and mono-bromobisphenol A, confirming the in-situ reductive debromination of TBBPA. Batch experiments showed that the removal of TBBPA was facilitated with S/Fe molar ratio of 0.2 and acidic conditions (pH = 3–7). The S-Fe^0/BC composite had good stability and reusability based on the cycle experiments. The removal process of TBBPA by S-Fe^0/BC composite might include chemical adsorption by S-Fe^0/BC composite, reduction debromination by S-Fe^0 and enhanced electron transfer. The environmentally-friendly S-Fe^0/BC composite synthesized by one-step facile procedure showed novel potential applications in terms of pollution control of halogenated xenobiotic compounds such as TBBPA.

* Corresponding author at: CAS Key Laboratory of Coastal Environmental Processes and Ecological Remediation, Yantai Institute of Coastal Zone Research (YIC), Chinese Academy of Sciences (CAS), Shandong Key Laboratory of Coastal Environmental Processes, YICCAS, Yantai, Shandong 264003, PR China.
E-mail address: jlu@yic.ac.cn (J. Lu).

1. Introduction

In the last decades, biochar has attracted much attention as a porous carbon material due to its porous structure, high specific surface area, low cost, and potential for carbon sequestration in the long run (Yao et al., 2013; Zhang et al., 2012). Seaweed is a favorable feedstock for biochar production, which has rich sources from land-based cultivation, ocean farms, or seaweed blooms that occur in aquatic environment (Duan et al., 2019; Lu et al., 2017; Yu et al., 2017). Since 2008, the frequent outbreak of green tide has become a major marine ecological disaster, accompany with millions tons of fresh *Ulva prolifera* (*U. prolifera*) beached on Shandong province (Zhang et al., 2019a, 2019b; Zhang et al., 2012). Excessive *U. prolifera* biomass has become a huge burden for both environmental and economic development in coastal areas. Therefore, it is of great practical significance to make full use of harmful seaweed biomass. Recently, the *U. prolifera*-based biochar through a rapid hydrothermal carbonization process was applied successfully to the adsorptive removal of endocrine-disrupting chemicals (EDCs), dyes, antibiotics and heavy metals (Lu et al., 2017; Ma et al., 2018; Yang et al., 2019). However, the adsorptive removal process achieved primarily by phase transfer, rather than transformed toxic pollutants into nontoxic or lower toxic substances. Hence, efforts must be endeavored to synthesize functionalized biochar possessing both adsorption and detoxification for environmental remediation.

Zero-valent iron (Fe^0) is a reductant with a large specific surface area and high reactivity. Standard redox potential of Fe^0 is low ($E = -0.44$ V) so that it can reduce many pollutants, such as metals, cyanide, antibiotics, phenol and nitrogen-containing heterocyclic compounds (He et al., 2019; Pirsaheb et al., 2019; Xu et al., 2020). However, Fe^0 easily forms aggregates and reacts with water or dissolved oxygen for forming an iron oxide cladding to make it passivate quickly, which limits its field application (Pirsaheb et al., 2019). More studies have reported that sulfidation could enhance electron availability and performance of Fe^0 toward certain halogenated xenobiotic compounds to enhance the removal efficiency of target pollutants such as trichloroethene (TCE) (Han and Yan, 2016; Mangayayam et al., 2019; Rajajayavel and Ghoshal, 2015), tetrabromobisphenol A (TBBPA) (Li et al., 2016a) and diclofenac (Song et al., 2017). However, S-nZVI alone is still facing the problem of easily air-oxidized, thereby reducing its reductive activity (Du et al., 2016). It is widely acknowledged that biochar can stabilize and disperse engineered particles, and thus enhance their mobility and stability (Peng et al., 2017). Fe modification has been proved to endow some algal-derived biochar with superior performance (Son et al., 2018). Thus, it can be assumed that the loading of sulfidated Fe^0 particles onto seaweed biochar could be a feasible method for better dispersion and higher reactivity, and thereafter exerting a synergistic effect that is not available from individual components.

Impregnation and precipitation are two main strategies that have been developed to synthesize Fe^0-based composite. However, both methods have some shortcomings such as the isolation of the biochar preparation from the iron-sulfur loading process (Han et al., 2019; Son et al., 2018), use of inorganic acid for washing the obtained pyrolyzed biochar material (Yang et al., 2018b; Zhu et al., 2018), and use of non-green reducing chemicals (e.g. sodium borohydride ($NaBH_4$)) for reducing the ferrous iron to zero-valent iron (Wu et al., 2018; Yang et al., 2018a). These disadvantages make the synthesis procedure expensive, complicated, time-consuming and environmentally unfriendly. Therefore, it is of great practical significance to establish a simple and green synthetic procedure for Fe^0/biochar composite.

In this study, magnetic *U. prolifera* biochar/sulfidated Fe^0 composite (S-Fe^0/BC) composite was synthesized through a simple one-step hydrothermal method which did not need to use non-green reducing chemicals (e.g. sodium borohydride ($NaBH_4$)) for reducing the ferrous iron to zero-valent iron. TBBPA, a fireproof additive, was selected as the target organic pollutant to test the performance of the S-Fe^0/BC

composite on the removal of harmful pollutants. TBBPA with lipophilicity and high octanol/water partition coefficient (log K_{ow} = 5.9) can be widely found in the organisms and various environmental media such as groundwater, soil and river sediments (Lin et al., 2012). Notably, TBBPA has been doubted to possess endocrine disruptor activity, which makes it toxic to organism (Decherf et al., 2010). The EDCs contamination has become a crucial stress affecting the sustainable development of the ecologically fragile regions such as the coastal zone (Lu et al., 2020a, 2020b). Therefore, it is an important issue to discuss the efficient removal of TBBPA and its toxicity reduction. The aims of this work are to: (1) establish a simple method for the preparation of S-Fe^0/BC composite; (2) investigate its performance on the removal of TBBPA; and (3) elucidate the underlying removal mechanisms of TBBPA by S-Fe^0/BC composite.

2. Materials and methods

2.1. Chemicals and materials

TBBPA (purity > 99%) was purchased from Dr. Ehrenstorfer GmbH (Augsburg, Germany) while bisphenol A (BPA, purity > 99%) was obtained from Sigma-Aldrich (St. Louis MO, USA). The trimethyl-chlorosilane (TMCS, purity > 98%) and N,O-bis(trimethylsilyl) trifluoroacetamide (BSTFA, purity > 98%) were supplied by Alfa Aesar (Ward Hill, MA). Dichloromethane and n-hexane with HPLC grade were obtained from Mreda (USA). Analytical reagents, such as ferrous sulfate heptahydrate ($FeSO_4·7H_2O$), sodium dithionite ($Na_2S_2O_4$), acetic acid (CH_3COOH), hydrochloric acid (HCl), and sodium hydroxide (NaOH) were all supplied by China National Medicines Co. (China). The stock solutions of TBBPA (1 g L^{-1}) were prepared by dissolving an appropriate amount of TBBPA in methanol in a volumetric flask and stored at -20 °C. The working solutions were gained by diluting stock solutions with deionized water to target concentration.

2.2. Preparation of S-Fe^0/BC and BC

The *U. prolifera* were collected on the beach of Rushan city, China. The fresh seaweed biomass was precleaned and grounded into slurry. For the preparation of S-Fe^0/BC, 2.98 g of $FeSO_4·7H_2O$ and 0.18 g of $Na_2S_2O_4$ powders were pre-dissolved in 30 mL of deoxygenated ultra-pure water, and well mixed with seaweed slurry (10 g). Further, the mixed slurry was transferred into a 100 mL stainless Teflon lined autoclave and placed in a tubular furnace at 180 °C for 4 h. After cooling to room temperature, the mixture was transformed to a 50 mL plastic centrifuge tube and centrifuged at 4200 rpm for 6 min to obtain the solid material. Afterwards, the material was washed three times with deoxyethanol to remove impurities before drying in a vacuum freeze-dryer (FD-1A-50, Boyikang, China). The obtained material was subsequently screened with a 60 mesh sieve and stored in vacuum bag for the following removal experiments. The final molar ratio of S/Fe was 0.2. Simultaneously, four more types of S-Fe^0/BC composites were prepared by varying the mass of $Na_2S_2O_4$ to produce composites with S/Fe ratios of 0, 0.1, 0.32, and 0.53, respectively. For comparison, the seaweed slurry (10 g) without addition of $FeSO_4·7H_2O$ and $Na_2S_2O_4$ were also conducted by the same procedure and labeled as BC.

2.3. Characterization

Surface morphologies and elemental distribution mapping were characterized by scanning electron microscopy (SEM; Hitachi S-4800, Japan) equipped with an energy dispersive spectrometer (EDS). The microstructure and morphology of the samples were examined by transmission electron microscopy (TEM; JEOL JEM-1400, Japan). The specific surface area was measured through the multipoint Brunauer-Emmett-Teller (BET) by adsorption of nitrogen at 77 K (ASAP 2000, Micromeritics Instrument Corp., Norcross, GA). The crystal structure of

the samples was carried out by X-ray diffraction (XRD, Bruker D8 Advance, Germany) at 40 mA and 40 kV over a range of 10–90° with Cu Kα radiation, λ = 1.5406 Å. The magnetic characterizations were performed using a vibrating sample magnetometry (VSM, Quantum Design VSM Versalab, USA). The functional groups of the synthesized materials were analyzed by Fourier transform infrared (FTIR, Nicolet IS10, USA). The surface components and their valance distributions on the surface of the materials were obtained by X-ray photoelectron spectroscopy (XPS, Thermo Scientific Escalab 250Xi, USA) with 150 W Al Kα radiation (h_v = 1486.6 eV). The binding energies were referenced to the C 1 s line at 284.8 eV from adventitious carbon.

2.4. TBBPA removal experiments

The batch experiments of TBBPA removal by the S-Fe^0/BC were conducted in 20 mL anaerobic blood culture bottles containing 15 mL reactive solution. The initial concentration of TBBPA was 1 mg L^{-1}, and the dosage of S-Fe^0/BC was 0.6 g L^{-1}. The TBBPA initial concentration was set as 1 mg L^{-1} based on previous investigations (Kang et al., 2018; Li et al., 2016a; Li et al., 2016b). The initial pH was 6.6 without any acid-base adjustment. The bottles were shaken at rolling speed of 180 rpm in darkness at room temperature (25 ± 0.5 °C). At given intervals, certain aliquots were sampled for TBBPA residual concentration analysis by ultra high performance liquid chromatography (UPLC). The products were also identified by gas chromatography-mass (GC/MS) spectrometry at the end of reaction. Two common kinetic models (i.e. pseudo first-order and pseudo second-order) and intraparticle diffusion model were applied to describe the removal kinetics of TBBPA. For comparison, TBBPA removal by BC material was conducted with the same procedure. Tap water spiked with TBBPA was also treated using S-Fe^0/biochar to test its application in real water treatment.

The equations of pseudo first-order kinetic model (Eq. (1)), pseudo second-order kinetic model (Eq. (2)) and intraparticle diffusion model (Eq. (3)) are shown as follows:

$$\ln(q_e - q_t) = \ln q_e - k_1 t \tag{1}$$

$$\frac{t}{q_t} = \frac{1}{k_2 q_e^2} + \frac{1}{q_e} t \tag{2}$$

$$q_t = k_i t^{0.5} + C \tag{3}$$

where q_e (mg g^{-1}) is the equilibrium adsorption capacity; k_1 (h^{-1}), k_2 (g (mg h)$^{-1}$) and k_i (mg g^{-1} h$^{1/2}$) are the rate constant of pseudo-first-order, pseudo-second-order and intraparticle diffusion adsorption, respectively; C is the intercept.

Additionally, various experimental setups were also conducted to investigate the influence of different variables such as dosage of S-Fe^0/BC (0.2, 0.4, 0.6, 1.2, and 2.4 g L^{-1}), initial TBBPA concentration (0.2, 0.5, 1, 2, 5, 10, and 20 mg L^{-1}), the S/Fe molar ratio of S-Fe^0/BC (0, 0.1, 0.2, 0.32, and 0.53) and pH (3.0–11.0) on the removal of TBBPA by S-Fe^0/BC. In this section, the TBBPA removal efficiency and adsorptive capacities rather than its removal rate during the 24 h period reaction was paid more attention. The TBBPA removal efficiency and adsorptive capacities were calculated based on Eq. (4) and (5), respectively.

$$\text{Removal}(\%) = \frac{C_0 - C_t}{C_0} \times 100\% \tag{4}$$

$$q_e = \frac{(C_0 - C_t)V}{m} \tag{5}$$

where C_0 (mg L^{-1}) is the initial concentration of TBBPA in liquid phase; C_t (mg L^{-1}) represents the TBBPA concentration in liquid phase at time t (h); V (L) is the volume of TBBPA solution used and m (mg) is the dosage of S-Fe^0/BC used.

To compare the performance of BC and S-Fe^0/BC on removal of TBBPA, the reusability of these two types of materials were tested.

Fresh BC and S-Fe^0/BC particles were added to react with TBBPA for 6 repetitive cycles. The reaction conditions were the same as the adsorptive experiments. In each cycle, 1 mL aliquots of reaction solution were collected from individual bottles after 24 h of reaction for the analysis of TBBPA residual concentration, and the remaining material was recovered through centrifugation at 4200 rpm for 15 min, which was then used for the next cycle of reaction.

2.5. Adsorptive isotherm experiment

To establish an adsorptive isotherm curve, temperature was regulated to 15 °C (288 K), 25 °C (298 K) and 35 °C (308 K) by shaker with initial TBBPA concentrations varying from 0.2 mg L^{-1} to 5 mg L^{-1}. Two classical adsorptive isotherm models, i.e. Langmuir model and Freundlich model were used for the mathematical description of TBBPA adsorption. The data were fitted according to the previous described method (Zhang et al., 2019a).

2.6. Analytical methods

The aqueous samples from the TBBPA batch experiments were immediately centrifuged at 12,000 rpm for 10 min. The residual concentrations of TBBPA in water samples were analyzed using a Waters ACQUITY UHPLC system (Milford, USA) equipped with a C$_{18}$ reverse phase column (2.1 × 50 mm, 1.7 μm). The mobile phase was acetonitrile/0.2% acetic acid solution (70/30, v/v %) with flow rate as 0.2 mL min^{-1}. The injection volume was 10 μL, and PDA detector at 210 nm.

For analysis of TBBPA transformation products, the samples before extracted products with liquid–liquid extraction (LLE) were centrifuged at 4200 rpm for 20 min to obtain the solid phase and the aqueous phase, respectively. The aqueous samples were extracted with 10 mL of CH$_2$Cl$_2$ for three times. The total of 30 mL of extract was concentrated to nearly dry by nitrogen evaporator, then redissolved with n-hexane (100 μL) and derivatized with BSTFA (containing 1% TMCS, 50 μL) at 70 °C for 2 h prior to GC/MS analysis. The derivatization of the TBBPA transformation products samples were analyzed using an Agilent 7820A GC system (Palo Alto, USA) coupled to a M7 single quadrupole MS system (Persee Co., China), equipping with a DB-5MS column (0.25 mm I.D, 30 m, Agilent J&W Scientific, USA). One microliter of the extract sample was injected in splitless mode with helium as a carrier gas. The temperature program for column oven was begun at 60 °C for 2 min, then increased to 210 °C with a 10 °C min^{-1} rate and kept for 3 min, continually increased to 290 °C with a 5 °C min^{-1} rate, and kept for 10 min. The total runtime was 46.00 min, including a solvent delay time of 7 min. The temperatures of ion source, the injector and transfer line were held at 230 °C, 280 °C and 250 °C, respectively.

2.7. Statistical analysis and data calculation

All experiments were conducted in triplicate. The results were processed using Origin 8.5 and IBM SPSS 20.0. One-way ANOVA followed by the Duncan test were applied to compare the differences of the TBBPA removal efficiency among various treatments. The statistical significance standard was weighed as $p < 0.05$.

3. Results and discussion

3.1. Characterization of magnetic S-Fe^0/BC particles

According to the SEM and TEM images, the BC possessed a porous structure and smoother surface, while S-Fe^0/BC composite had a spherical shape with a particle size in the range from 200 to 850 nm and unevenly distributed on the biochar surface and inside the pores. The EDS spectrum of the selected region of BC showed an O/C atomic ratio of 0.33, representing a typical biochar matrix. For S-Fe^0/BC composite,

high Fe (13.47%) and S (1.29%) atomic percentages indicated a successful modification of Fe and S on the surface of BC. Meanwhile, elemental mapping of C, Fe and S distribution pattern proved the formation of sulfide-modified Fe^0 distribution throughout the biochar matrix. The disagreement of Fe and O distribution pattern suggested the existence of iron oxides and Fe^0. The specific surface area of S-Fe^0/BC (47.2 m^2 g^{-1}) was significantly higher than that of BC (25.4 m^2 g^{-1}) based on the BET analysis, which was attributed to the burden of a large number of particles on BC surface or even its channel. Additionally, the phase composition of the S-Fe^0/BC composite was characterized by XRD. The position of the 2θ angle at 25.2° displayed a diffraction peak, which is a typical peak of graphitized microcrystalline carbon (0 0 2) after carbonization (Zheng et al., 2016). Two sharp peaks were observed in the S-Fe^0/BC composite with the 2θ angles at 44.68° and 65.03°, corresponding to the (1 1 0) and (2 0 0) crystal faces of α-Fe, indicating the presence of Fe^0 in the composite (Du et al., 2016). Magnetic hysteresis loops presented that the S-Fe^0/BC composite exhibited high coercivity (59 Oe) and large saturation magnetization (41.11 emu g^{-1}) while BC had saturation magnetization less than 1.5 emu g^{-1} to represent for a near-zero magnetization. The ferromagnetic properties of S-Fe^0/BC provided a green separation method for exhausted material recycling.

3.2. The performances of S-Fe^0/BC on TBBPA removal

The initial TBBPA concentration with 1 mg L^{-1} was used to test the removal potential of S-Fe^0/BC. As it was displayed in Fig. 1a, the removal efficiency of TBBPA by S-Fe^0/BC composite treatment within 24 h was 88.2%, which was much higher than that in BC treatment (55.3%) in deionized water system, indicating that the modification by sulfide and iron on seaweed-based biochar could be an effective method to enhance TBBPA removal. Additionally, the TBBPA removal efficiency by S-Fe^0/BC composite could also exceed 80% in the tap water spiking experiment, suggesting a potential further application for S-Fe^0/BC composite in real water. Simultaneously, the removal rate of TBBPA by S-Fe^0/BC composite in deionized water system was observed to increase rapidly within 12 h, and then slow down until equilibrium with the removal capacity as 1.47 mg g^{-1}. In order to better describe the removal process of TBBPA by BC and S-Fe^0/BC composite, the kinetic data were fitted using pseudo-first and pseudo-secondary kinetic models. As it was illustrated in Fig. 1b, the first-order kinetic model fitted well ($R^2 > 0.99$) with the rate constant k_{BC-1} of 0.15 h^{-1} for the BC material. For the S-Fe^0/BC composite, the pseudo-second-kinetic model fitting results ($R^2 = 0.99$) were better than that of pseudo-first-order kinetic model ($R^2 = 0.94$) and the rate constant $k_{S-Fe0/BC-2}$ was 0.98 h^{-1}. These results indicated that the removal of TBBPA by BC was mainly physical adsorption under electrostatic action, while the rate-limited process of TBBPA removal by S-Fe^0/BC composite was a chemical process. Considering that the TBBPA removal mechanism by S-Fe^0/BC composite was more complicated than that by BC, the intraparticle diffusion model was then applied. According to Fig. 1c, a sharp slope (k_{a1} = 0.67 mg/g $h^{-1/2}$) was displayed in the first stage when the TBBPA molecules were transported from solution onto the external surface of S-Fe^0/BC composite. Simultaneously, chemical adsorptions of electron transfer occurred in this stage. Hereafter, the intraparticle diffusion and inner sites adsorption were started in the following stages with lower rate (k_{a2} = 0.17 mg/g $h^{-1/2}$ and k_{a3} = 0.02 mg/g $h^{-1/2}$) and served as the limiting step.

3.3. Effect of S/Fe molar ratio on TBBPA removal

During synthesis of S-Fe^0/BC composite, the S/Fe molar ratio in initial solution phase determined the sulfidation extent of the materials and thereby may influence the removal efficiency of target compounds. To evaluate the effect of S/Fe molar ratio on TBBPA removal, S-Fe^0/BC with different S/Fe molar ratio (0, 0.1, 0.2, 0.32, and 0.53) was
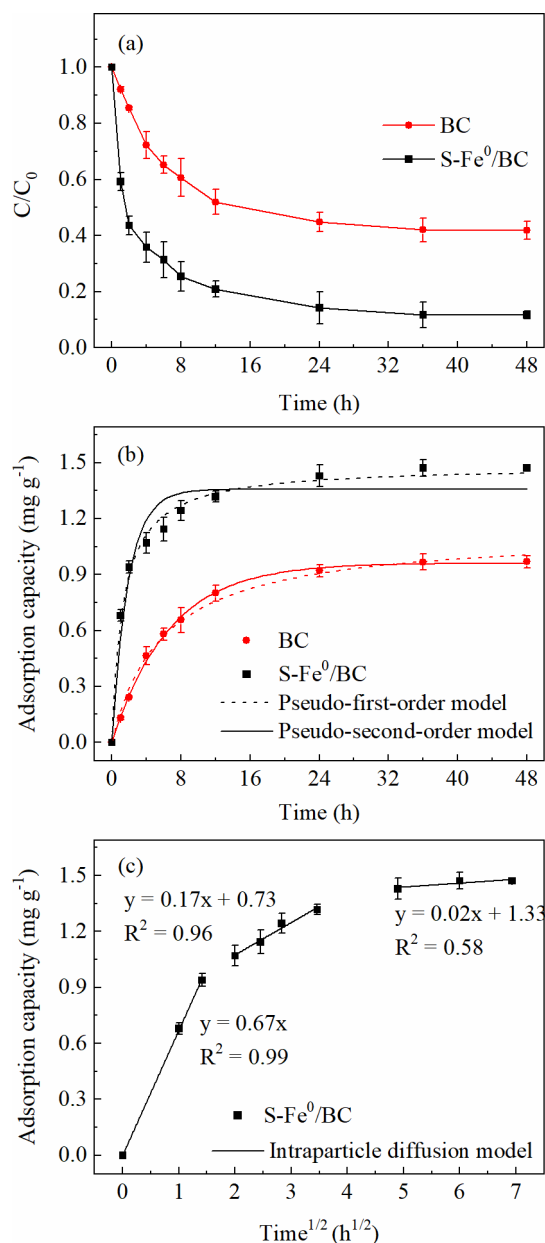

Fig. 1. The removal efficiency of TBBPA as a function of time by BC and S-Fe^0/BC (a), pseudo-first-order and pseudo-second-order model fitting curves for TBBPA removal by BC and S-Fe^0/BC (b), and intraparticle diffusion model fitting curves by S-Fe^0/BC (c).

prepared (Fig. 2a). In general, the adsorptive capacities of TBBPA increased initially, and then decreased with the increasing S/Fe molar ratio. The highest TBBPA adsorptive capacities was achieved at S/Fe ratio = 0.2 (1.47 mg g^{-1}), which was much higher than that in the treatment without sulfidation (S/Fe ratio = 0). This phenomenon indicated that sulfidation was beneficial to the removal of contaminant. However, too high S/Fe ratio also hampered the TBBPA removal. As the S/Fe ratio increasing to 0.53, the TBBPA adsorptive capacities dropped dramatically by 23%. The difference in adsorptive capacities of various molar ratios of S/Fe could be attributed to the different extent of sulfidation (Su et al., 2015). Sulfidation inhibited the aggregation of Fe^0 and facilitated the surface contact between pollutants and Fe^0 to some extent (Song et al., 2017). However, FeS layer covering on the surface of Fe^0 becomes more extensive and secondary FeS layers might form with higher S/Fe molar ratio (Fan et al., 2017), which may seriously inhibit corrosion of Fe^0 to subsequently show an adverse effect on
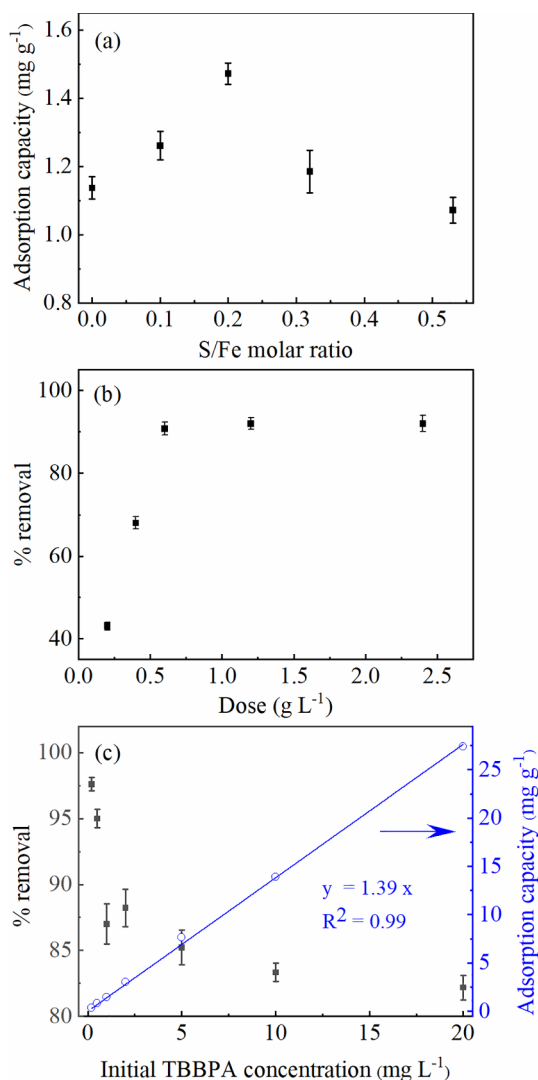
Fig. 2. The effects of S/Fe molar ratio (a), dosage of S-Fe^0/BC (b) and initial TBBPA concentration (c) on the removal efficiency of TBBPA by S-Fe^0/BC.

TBBPA removal. Additionally, the excessive amount of sulfur might generate polysulfide compounds (S_n^{2-}), which has a lower reactivity than FeS (Han and Yan, 2016).

3.4. The effects of the dosage of S-Fe^0/BC composite and the initial concentration of TBBPA on TBBPA removal

The effect of the dosage of S-Fe^0/BC composite (S/Fe ratio = 0.2) on the degradation of TBBPA was studied under the initial concentration of TBBPA as 1 mg L^{-1}. The TBBPA removal efficiency increased from 43.0% to 88.2% when the dosage of S-Fe^0/BC composite increased from 0.2 g L^{-1} to 0.6 g L^{-1} (Fig. 2b), indicating that S-Fe^0/BC composite had high performance on TBBPA removal. The main reason might be that higher dose of S-Fe^0/BC had a larger specific surface area to provide more adsorption and chemical reaction sites (Li et al, 2016a). O'Carroll et al. (2013) found that Fe^0 materials in a certain dosage range could promote the degradation of pollutants, while excessive Fe^0 dosage reduced the removal efficiency of target pollutant due to the agglomeration of nanoparticles. However, *U. prolifera*-based biochar as the supporter of S-Fe^0 avoided this disadvantage. When the amount of S-Fe^0/BC material was more than 1.2 g L^{-1}, the degradation

efficiency of TBBPA was still kept above 92%.

The initial concentration provides an important driving force to overcome all mass transfer resistances of the target contaminants between the aqueous and solid phases. Fig. 2c showed the influence of initial TBBPA concentration with the S-Fe^0/BC composite dosage of 0.6 g L^{-1}. Although the removal efficiency of TBBPA decreased from 97.6% to 82.1% as the initial concentration increased from 0.2 to 20 mg L^{-1}, the removal capacity of TBBPA linearly increased from 0.33 to 27.4 mg g^{-1}, which was comparable or higher than other reported adsorption material (Kang et al., 2018; Ren et al., 2019; Zhou et al., 2019). For instance, Kang et al. (2018) reported that the removal capacity for TBBPA was about 10 mg g^{-1} by Au/Fe@ biocarbon with initial TBBPA concentration of 10 mg L^{-1} under 303 K. However, the synthesis of such materials generally needed high-cost raw materials, extra iron loading process for isolating the biochar, and usage of non-green reducing materials (e.g. sodium borohydride (NaBH$_4$)) for reducing the ferrous iron to zero-valent iron. Hence, S-Fe^0/BC composite synthesized by one-pot method could be a promising material in terms of pollution control of halogenated xenobiotic compounds due to its low cost, time-consuming and environmentally unfriendly.

3.5. The effect of pH on TBBPA removal

The coastal environments could be subjected to fluctuations in pH, which may alter the adsorptive removal of organic pollutant on S-Fe^0/BC composite. The effect of pH on the TBBPA removal capacity was displayed in Fig. 3a. Overall, the adsorptive capacity of TBBPA by S-Fe^0/BC decreased with increasing initial pH from 4 to 11. TBBPA was
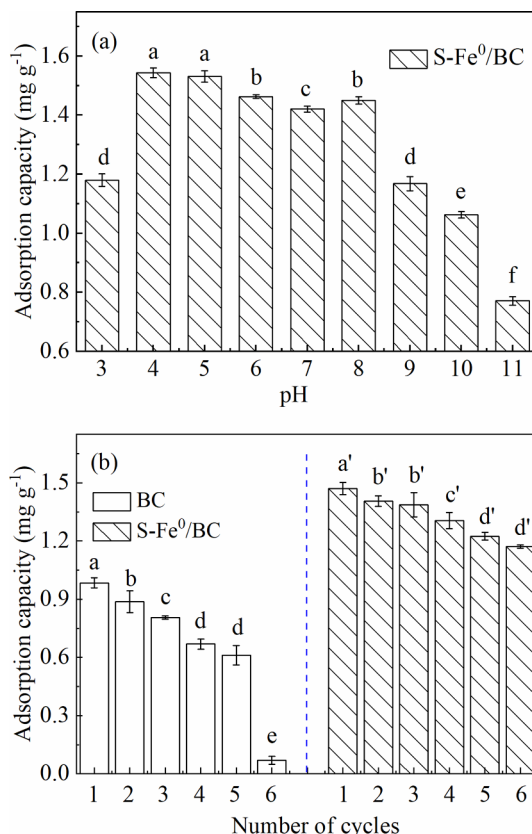

Fig. 3. The effect of pH on the removal capacity of TBBPA by S-Fe^0/BC (a) and the effect of number of cycles on the removal capacity of TBBPA by BC and S-Fe^0/BC (b). The different letters at the top of the histogram indicate a significant difference (p < 0.05) in TBBPA removal capacity, and the same letter manifests no significant difference in removal capacity (p > 0.05).

easily removed under neutral or acidic pH conditions (pH = 4–7), and its concentration dropped dramatically from 1.47 mg g^{-1} to 0.77 mg g^{-1} when the initial pH increased from 8.0 to 11.0. It is well-known that Fe^0 dissolution strongly depends on pH. Under acid conditions, the TBBPA removal capacity would increase markedly since the content of H$^+$ was sufficient to destroy the passivation layers and form corrosion pits on the surface of Fe^0, which would favor electron transferring (Wu et al., 2018). However, it must be noted that the amount of TBBPA removed also decreased sharply under extreme acidic conditions (i.e. pH = 3). A reasonable explanation was that the electrons (e$^-$) were rapidly consumed by H$^+$ to form H$_2$, rather than transformed to TBBPA under extremely acidic conditions. Li et al. (2016b) also found that the extreme acid environment would decrease the removal efficiency of organic compound by Ni/nZVI bimetallic particles, and supposed that small H$_2$ bubbles forming on the surface might act as a barrier that prevented the contact of target pollutant to Ni/nZVI surface. In alkaline conditions, the decrease of TBBPA removal capacity might be ascribed to the ferrous ions released during the corrosion of the material. The ferrous ions could collide with the hydroxide ions to cause precipitation of ferrous hydroxide on the S-Fe^0/BC surface, and thereafter occupy the reaction sites (Lin et al., 2012). Notably, the pH of wastewater usually ranged from 5.5 to 9 (Wang et al., 2015), with which more than 65% of TBBPA removal efficiency could be achieved, suggesting that the S-Fe^0/BC is a potential material for TBBPA removal from the wastewater under wide pH conditions.

3.6. The reusability of S-Fe^0/BC material

There is no doubt that reusability is one of the most important factors determining the applicability of materials for the removal of pollutants. In this study, cycle experiment was conducted to observe the reusability of S-Fe^0/BC material with the BC material used as a control. The adsorptive capacity of TBBPA by both BC and S-Fe^0/BC was shown in Fig. 3b. In the first cycle, the removal capacity of TBBPA by S-Fe^0/BC was 1.45 mg g^{-1}, with about 47% enhancement than that of BC. The TBBPA removal efficiency in the S-Fe^0/BC system kept constant initially with increased cycles and showed a small decline after third cycles, while that in the BC system dropped continuously. After the sixth cycle, the removal capacity on S-Fe^0/BC still maintained more than 1.17 mg g^{-1} while that on BC was below 0.07 mg g^{-1}, indicating that iron-sulfur treatment of algal-based biochar could improve the reusability and longevity of seaweed biochar. The sulfidation could effectively inhibit iron oxidation and corrosion of Fe^0 and improve the electron availability to contaminants, hence improving reusability of S-Fe^0/BC composite observed in this study. On the other hand, biochar might act as an efficient carrier for the S-Fe^0 particles and "electron shuttle" that transforms electrons from the Fe^0 and FeS to the target compound (Dong et al., 2017). However, the decrease in TBBPA removal efficiency was mainly caused by the gradual consumption of S-Fe^0 and the occupation of adsorptive sites on biochar. For the BC material, the TBBPA removal mainly depended on its physical adsorptive process, and the limitation of adsorptive sites and surface functional groups led to the saturation of TBBPA adsorption capacity. Therefore, S-Fe^0/BC composite might be a promising candidate for the treatment of actual polluted water environment.

3.7. Proposed degradation mechanism

In the reaction system of S-Fe^0/BC, the products in both aqueous phase and solid phase after 24 h reaction were extracted and detected by GC/MS. Besides the peak (37.334 min) of TBBPA, the peaks of bisphenol A (BPA) and monobromobisphenol A (mono-BBPA) appeared at 24.155 min and 29.816 min in aqueous phase, confirming in-site

reductive debromination of TBBPA. Interestingly, mono-BBPA and BPA were also detected in the GC/MS chromatogram extracted from S-Fe^0/BC solid phase and the peak area of both products on solid phase is much higher than that in aqueous phase. In order to estimate the distribution of target pollutants between two phases, the S-Fe^0/BC-water partition coefficients (k_{sw}) of the mono-BBPA and BPA were calculated based on the ratios of peak area of two products on S-Fe^0/BC and that in the medium. The k_{sw} was calculated as 8.9 for mono-BBPA and 1.8 for BPA, indicating that the degradation products of TBBPA were incline to enrich on the surface of S-Fe^0/BC, which may beneficial to their further removal from water. Previous studies using other iron-based nanomaterials (e.g. S-Fe^0 and Ni/Fe^0) also proposed that TBBPA could undergo a continuous debromination pathway to form a stepwise debromination product (Li et al., 2016a; Li et al., 2016b). However, tribromobisphenol A (tri-BBPA) and dibromobisphenol A (di-BBPA) were not found in this study, most likely due to their low concentration in the reaction system. The results demonstrated that S-Fe^0/BC composite was a promising material due to its thorough reduction of TBBPA and in-situ formation of BPA, which possess lower thyroid hormonal-disrupting activity (Kitamura et al., 2002).

FTIR and XPS characterization were evaluated to further understand the change in functional groups and surface valence state of S-Fe^0/BC composite before and after reactions with TBBPA for six cycles. The FTIR spectrum showed that bounded TBBPA caused slight shifts in stretching band and increased frequencies of surface functional groups such as –OH (from 3358 to 3388 cm^{-1}), –CH$_2$ (from 2922 to 2920 cm^{-1}), C = O (1697 cm^{-1}), C = C/N–H (from 1629 to 1625 cm^{-1}), and aromatic C–H (from 801 to 796 cm^{-1}), indicating that TBBPA was integrated on the seaweed biochar through interactions with these functional groups (Dong et al., 2017; Lu et al., 2017). The bands between 900 cm^{-1} and 460 cm^{-1} could be assigned to the Fe-O bending vibrations with different species of iron oxides (Yang et al., 2018b; Zhao et al., 2020). The enhancement of intensity at 796 cm^{-1} after reaction indicated that the formation of more iron oxides after reaction, and the characteristic peak at 598 cm^{-1} implied the formation of Fe$_3$O$_4$ (Mandal et al., 2020), which showed a slight weaken after reaction with TBBPA for six cycles. Additionally, the intensity enhancement and wavenumber shift of S-O vibrations (from 1126 cm^{-1} to 1103 cm^{-1}) indicated that iron sulfide was oxidized to form more SO$_4{}^{2-}$ (Dong et al., 2018). The results will be further discussed together with XPS to elucidate the possible mechanisms of TBBPA removal by the S-Fe^0/BC composite.

XPS survey was performed for Fe, S and Br species to clarify the valence change of surface elements before and after reaction for six cycles with TBBPA. Four peaks occurred in Fe spectrum, which corresponded to Fe^0 (707.2 eV), FeO (710.1 eV), FeS (711.3 eV), and Fe$_3$O$_4$ (712.9 eV) species. Compared with the 0 h reaction, reaction for six cycles led to more obvious weakened peaks for Fe^0, and strengthened peaks for FeS. This suggested that the surface of Fe^0 particles were enclosed by a thin layer of iron oxide or iron sulfide. The presence of iron oxides on the Fe^0 particle surfaces is unsurprising given their high reactivity in contact with oxygen. The S 2p spectrum of S-Fe^0/BC displayed three peaks at 161.9 eV, 163.8 eV and 168.5 eV, which was supposed to the S^{2-}, S$_n{}^{2-}$ and SO$_4{}^{2-}$ species, respectively. The S 2p spectrum showed a weakened peak for S^{2-} and strengthened peaks for S$_n{}^{2-}$ after reaction with TBBPA for six cycles, confirming the consumption of S^{2-} reacted with TBBPA. Additionally, FeS was proved to possess excellent electrical conductivity compared with iron oxides (Fan et al., 2017). Therefore, the enhanced electron transfer between FeS on S-Fe^0/BC surface and the adsorbed TBBPA facilitated the reduction of TBBPA. The XPS scan of Br 3d for used material showed two new peaks at 68.5 eV and 70.4 eV, assigning to C-Br and Br$^-$, respectively. The presence of C-Br demonstrated of TBBPA adsorption on the
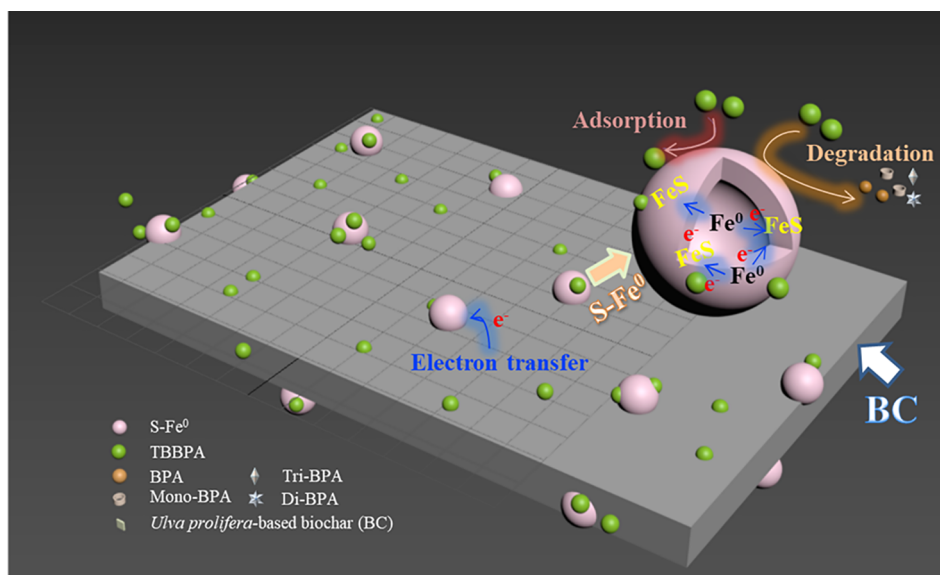
Fig. 4. Proposed reaction mechanisms for the removal of TBBPA by S-Fe^0/BC.

surface of biochar. Moreover, the detection of Br$^-$ further confirmed the in-suit reductive debromination of TBBPA.

Taken together, removal of TBBPA by S-Fe^0/BC materials might undergo multiple processes, mainly including chemical adsorption, subsequent reduction removal, and enhanced electron transfer (Fig. 4). The porous support material (BC) not only promoted TBBPA adsorption relying on its large specific surface area and rich functional groups, but also enhanced TBBPA reduction by transforming electrons from the Fe^0 and FeS to the target compound. The exact mechanisms on degradation of contaminant using these electrons were not clear. However, it could be assumed that both the seaweed biochar and iron atoms in the iron sulfide molecule could act as a transmitter conveying electrons from the surrounding sulfur atoms to the halo compounds (Dong et al., 2017). Simultaneously, Fe^0 and FeS supported on biochar also possessed large specific surface area and thus enhanced surface adsorption capacity for TBBPA molecules. The TBBPA adsorbed on the surface of S-Fe^0/BC could react with Fe^0 and FeS further, which was the degradation process of TBBPA. Additionally, the enhanced electron transfer between FeS on S-Fe^0/BC surface and the adsorbed TBBPA facilitated the reduction of TBBPA. In general, simultaneous adsorption-reduction of TBBPA by S-Fe^0/BC composite was achieved due to the synergistic effect between BC, Fe^0, and FeS.

3.8. Adsorption isotherms

Adsorption isotherms were applied to describe the partition process of TBBPA molecular between liquid and solid phase under different temperatures. Compared with the Langmuir model, the Freundlich model fitted the experimental data well by both BC and S-Fe^0/BC composite (Fig. 5). The correlation coefficients (R^2) of Freundlich model by BC was ranged from 0.97 to 0.98, while that by S-Fe^0/BC composite was from 0.98 to 0.99. It is well understood that the Freundlich model was applicable to a heterogeneous surface with adsorption sites possessing different adsorption energies, while Langmuir model is more capable of a uniform surface with limited number of adsorption sites. These indicated that the adsorbent (S-Fe^0/BC composite) surface was more heterogeneous after modified by sulfur and iron. K_F and $1/n$ are two Freundlich constants, which related to the adsorption capacity and adsorption intensity. The values of K_F showed an

obvious enhancement as the rise of temperature for TBBPA removal by S-Fe^0/BC composite (Fig. 5 inset) and the maximum K_F value was determined as 22.61 L g^{-1} at 308 K, indicating that the adsorptive process was endothermic. Simultaneously, n values (ranged from 1.15 to 1.19) were greater than unity, indicating that the TBBPA were favorably partitioning into S-Fe^0/BC composite (Zhou et al., 2019). Notable, the isotherms of the TBBPA implied no saturation within the initial TBBPA concentration (0.2–5 mg L^{-1}) and temperature ranges (288–308 K), manifesting that a complete monolayer of TBBPA covering has not formed on the surface of BC and S-Fe^0/BC composite.

4. Conclusions

A time-saving and environmentally-friendly synthetic process for magnetic S-Fe^0/BC composite was provided. Enhanced TBBPA removal efficiency by S-Fe^0/BC composite was realized through chemical adsorption by S-Fe^0/BC composite, reduction debromination by S-Fe^0, and enhanced electron transfer. S/Fe molar ratio of 0.2 and acidic conditions (pH = 3–7) facilitated the removal of TBBPA. Good magnetism and reusability further demonstrated that S-Fe^0/BC composite possessed novel potential in pollution control of halogenated xenobiotic compounds such as TBBPA.

CRediT authorship contribution statement

Cui Zhang: Investigation, Formal analysis, Data curation, Methodology, Writing - original draft. **Jian Lu:** Conceptualization, Funding acquisition, Project administration, Supervision, Writing - review & editing. **Jun Wu:** Investigation, Methodology, Writing - review & editing.

Declaration of Competing Interest

The authors declare that they have no known competing financial interests or personal relationships that could have appeared to influence the work reported in this paper.
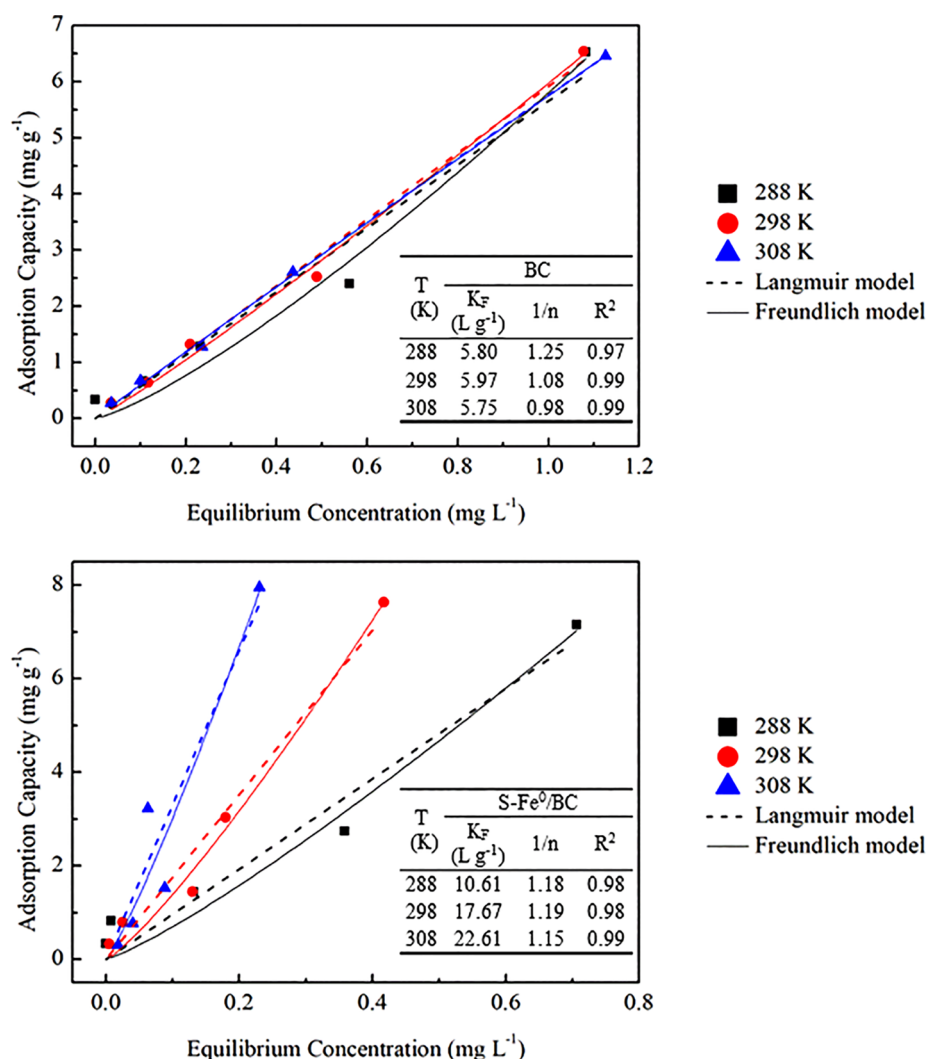
T (K)	BC		
	K_F (L g^{-1})	1/n	R^2
288	5.80	1.25	0.97
298	5.97	1.08	0.99
308	5.75	0.98	0.99

T (K)	S-Fe^0/BC		
	K_F (L g^{-1})	1/n	R^2
288	10.61	1.18	0.98
298	17.67	1.19	0.98
308	22.61	1.15	0.99

Fig. 5. Adsorptive isotherms of TBBPA on BC (a) and S-Fe^0/BC (b) at different temperatures. Inset: Freundlich adsorption isotherm constants for the adsorption of TBBPA at different temperature.

Acknowledgements

Appendix A. Supplementary data

Supplementary data to this article can be found online at https://doi.org/10.1016/j.biortech.2020.123170.

References

Decherf, S., Seugnet, I., Fini, J.B., Clerget-Froidevaux, M.S., Demeneix, B.A., 2010. Disruption of thyroid hormone-dependent hypothalamic set-points by environmental contaminants. Mol. Cell. Endocrinol. 323 (2), 172–182.

Dong, H., Cong, Z., Hou, K., Cheng, Y., Deng, J., Zhao, J., Lin, T., Zeng, G., 2017. Removal of trichloroethylene by biochar supported nanoscale zero-valent iron in aqueous solution. Sep. Purif. Technol. 188, 188–196.

Dong, H., Zhang, C., Deng, J., Jiang, Z., Zhang, L., Cheng, Y., Hou, K., Tang, L., Zeng, G.,

2018. Factors influencing degradation of trichloroethylene by sulfide-modified nanoscale zero-valent iron in aqueous solution. Water Res. 135, 1–10.

Du, J.K., Bao, J.G., Lu, C.H., Werner, D., 2016. Reductive sequestration of chromate by hierarchical FeS@Fe^0 particles. Water Res. 102, 73–81.

Duan, X., Chen, Y.Z., Yan, Y.Y., Feng, L.Y., Chen, Y.G., Zhou, Q., 2019. New method for algae comprehensive utilization: Algae-derived biochar enhances algae anaerobic fermentation for short-chain fatty acids production. Bioresour. Technol. 289, 121637.

Fan, D., Lan, Y., Tratnyek, P.G., Johnson, R.L., Filip, J., O'Carroll, D.M., Nunez Garcia, A., Agrawal, A., 2017. Sulfidation of iron-based materials: A review of processes and implications for water treatment and remediation. Environ. Sci. Technol. 51 (22), 13070–13085.

Han, B., Song, L., Li, H., Song, H., 2019. Naked oats biochar-supported nanoscale zero-valent iron composite: effects on Cd immobilization and enzyme activities in Ulansuhai River sediments of China. J. Soil. Sediment. 19 (5), 2650–2662.

Han, Y.L., Yan, W.L., 2016. Reductive dechlorination of trichloroethene by zero-valent iron nanoparticles: Reactivity enhancement through sulfidation treatment. Environ. Sci. Technol. 50 (23), 12992–13001.

He, C., Lin, W., Zheng, X., Wang, C., Hu, Z., Wang, W., 2019. Synergistic effect of magnetite and zero-valent iron on anaerobic degradation and methanogenesis of phenol. Bioresour. Technol. 291, 121874.

Kang, N., Zhu, H., Guo, W., Shi, C., Wu, P., Wei, X., 2018. Efficient debromination of Tetrabromobisphenol A (TBBPA) by Au/Fe@biocarbon derived from bioreduction precious metals. Chem. Eng. J. 334, 99–107.

Kitamura, S., Jinno, N., Ohta, S., Kuroki, H., Fujimoto, N., 2002. Thyroid hormonal activity of the flame retardants tetrabromobisphenol A and tetrachlorobisphenol A. Biochem. Biophys. Res. Co. 293 (1), 554–559.

Li, D., Mao, Z., Zhong, Y., Huang, W., Wu, Y., Peng, P.A., 2016a. Reductive transformation of tetrabromobisphenol A by sulfidated nano zerovalent iron. Water Res. 103, 1–9.

Li, Y., Li, X., Yang, X., Wei, C., Han, D., Huang, W., 2016b. Catalytic debromination of tetrabromobisphenol A by Ni/nZVI bimetallic particles. Cheml. Eng. J. 284, 1242–1250.

Lin, K., Ding, J., Huang, X., 2012. Debromination of tetrabromobisphenol A by nanoscale zerovalent iron: Kinetics, influencing factors, and pathways. Ind. Eng. Chem. Res. 51 (25), 8378–8385.

Lu, J., Wu, J., Zhang, C., Zhang, Y., 2020a. Possible effect of submarine groundwater discharge on the pollution of coastal water: Occurrence, source, and risks of endocrine disrupting chemicals in coastal groundwater and adjacent seawater influenced by reclaimed water irrigation. Chemosphere 250, 126323.

Lu, J., Zhang, C., Wu, J., Luo, Y., 2017. Adsorptive removal of bisphenol A using N-doped biochar made of *Ulva Prolifera*. Water Air Soil Pollut. 228 (9), 327.

Lu, J., Zhang, C., Wu, J., Zhang, Y., Lin, Y., 2020b. Seasonal distribution, risks, and sources of endocrine disrupting chemicals in coastal waters: Will these emerging contaminants pose potential risks in marine environment at continental-scale? Chemosphere 247, 125907.

Ma, Y., Wang, J., Zhang, Y., 2018. 'Green tide' to biochar: preparation and adsorption isotherms for three typical organic pollutants. Prog. React. Kinet. Mech. 43 (1), 30–40.

Mandal, S., Pu, S., Shangguan, L., Liu, S., Ma, H., Adhikari, S., Hou, D., 2020. Synergistic construction of green tea biochar supported nZVI for immobilization of lead in soil: A mechanistic investigation. Environ. Int. 135, 105374.

Mangayayam, M., Perez, J.P., Dideriksen, K., Freeman, H., Nano, D.T.J.E.S., 2019. Structural transformation of sulfidized zerovalent iron and its impact on long-term reactivity. Environ. Sci.: Nano. 6 (11), 3422–3430.

O'Carroll, D., Sleep, B., Krol, M., Boparai, H., Kocur, C., 2013. Nanoscale zero valent iron and bimetallic particles for contaminated site remediation. Adv. Water Resour. 51 (1), 104–122.

Peng, X., Liu, X., Zhou, Y., Bo, P., Lin, T., Lin, L., Yao, B., Deng, Y., Jing, T., Zeng, G., 2017. New insights into the activity of a biochar supported nanoscale zerovalent iron composite and nanoscale zero valent iron under anaerobic or aerobic conditions. RSC Adv. 7 (15), 8755–8761.

Pirsaheb, M., Moradi, S., Shahlaei, M., Wang, X., Farhadian, N., 2019. A new composite of nano zero-valent iron encapsulated in carbon dots for oxidative removal of bio-refractory antibiotics from water. J. Clean. Prod. 209, 1523–1532.

Rajajayavel, S.R., Ghoshal, S., 2015. Enhanced reductive dechlorination of trichloroethylene by sulfidated nanoscale zerovalent iron. Water Res. 78, 144–153.

Ren, L., Li, L., Chen, S., Li, H., Liu, Y., Zhou, L., Guo, S., Yu, Y., 2019. Yolk-shell Fe/FeS@SiO$_2$ particles with enhanced dispersibility, transportability and degradation of TBBPA. Catal. Today 327, 2–9.

Son, E.-B., Poo, K.-M., Chang, J.-S., Chae, K.-J., 2018. Heavy metal removal from aqueous solutions using engineered magnetic biochars derived from waste marine macro-algal biomass. Sci. Total Environ. 615, 161–168.

Song, S.K., Su, M.M., Adeleye, A.S., Zhang, Y.L., Zhou, X.F., 2017. Optimal design and characterization of sulfide-modified nanoscale zerovalent iron for diclofenac removal. Appl. Catal. B: Environ. 201, 211–220.

Su, Y., Adeleye, A.S., Keller, A.A., Huang, Y., Dai, C., Zhou, X., Zhang, Y., 2015. Magnetic sulfide-modified nanoscale zerovalent iron (S-nZVI) for dissolved metal ion removal. Water Res. 74, 47–57.

Wang, Y., Lu, J., Wu, J., Liu, Q., Zhang, H., Jin, S., 2015. Adsorptive removal of fluoroquinolone antibiotics using bamboo biochar. Sustainability. 7 (9), 12947.

Wu, H., Feng, Q., Yang, H., Lu, P., Gao, B., Alansari, A., 2018. Enhanced phenanthrene removal in aqueous solution using modified biochar supported nano zero-valent iron. Environ. Technol. 132067, 1–30.

Xu, W., Zhao, H., Cao, H., Zhang, Y., Sheng, Y., Li, T., Zhou, S., Li, H., 2020. New insights of enhanced anaerobic degradation of refractory pollutants in coking wastewater: Role of zero-valent iron in metagenomic functions. Bioresour. Technol. 300, 122667.

Yang, F., Zhang, S., Sun, Y., Cheng, K., Li, J., Tsang, D.C.W., 2018a. Fabrication and characterization of hydrophilic corn stalk biochar-supported nanoscale zero-valent iron composites for efficient metal removal. Bioresour. Technol. 265, 490–497.

Yang, F., Zhang, S.S., Li, H.P., Li, S.S., Cheng, K., Li, J.S., Tsang, D.C.W., 2018b. Corn straw-derived biochar impregnated with α-FeOOH nanorods for highly effective copper removal. Cheml. Eng. J. 348, 191–201.

Yang, W., Wang, Z., Song, S., Han, J., Chen, H., Wang, X., Sun, R., Cheng, J., 2019. Adsorption of copper(II) and lead(II) from seawater using hydrothermal biochar derived from *Enteromorpha*. Mar. Pollut. Bull. 149, 110586.

Yao, H., Lu, J., Wu, J., Lu, Z.Y., Wilson, P.C., Shen, Y., 2013. Adsorption of fluoroquinolone antibiotics by wastewater sludge biochar: Role of the sludge source. Water Air Soil Pollut. 224 (1), 1370.

Yu, K.L., Lau, B.F., Show, P.L., Ong, H.C., Ling, T.C., Chen, W.H., Ng, E.P., Chang, J.S., 2017. Recent developments on algal biochar production and characterization. Bioresour. Technol. 246, 2–11.

Zhang, C., Lu, J., Wu, J., 2019a. Adsorptive removal of polycyclic aromatic hydrocarbons by detritus of green tide algae deposited in coastal sediment. Sci. Total Environ. 670, 320–327.

Zhang, C., Lu, J., Wu, J., Luo, Y., 2019b. Phycoremediation of coastal waters contaminated with bisphenol A by green tidal algae *Ulva prolifera*. Sci. Total Environ. 661, 575–582.

Zhang, Z., Wang, K., Atkinson, J.D., Yan, X., Li, X., Rood, M.J., Yan, Z., 2012. Sustainable and hierarchical porous *Enteromorpha prolifera* based carbon for CO$_2$ capture. J. Hazard. Mater. 229–230, 183–191.

Zhao, J., Yang, X., Liang, G., Wang, Z., Li, S., Wang, Z., Xie, X., 2020. Effective removal of two fluoroquinolone antibiotics by PEG-4000 stabilized nanoscale zero-valent iron supported onto zeolite (PZ-NZVI). Sci. Total Environ. 710, 136289.

Zheng, Q.F., Wang, Z.M., Chen, B.G., Liu, G.F., Zhao, J., 2016. Analysis of XRD spectral structure and carbonization of the biochar preparation. Spectrosc. Spect. Anal. 36 (10), 3355–3359.

Zhou, Q., Wang, Y., Xiao, J., Zhan, Y., 2019. Preparation of magnetic core-shell Fe$_3$O$_4$@polyaniline composite material and its application in adsorption and removal of tetrabromobisphenol A and decabromodiphenyl ether. Ecotox. Environ. Safety 183, 109471.

Zhu, S., Huang, X., Wang, D., Wang, L., Ma, F., 2018. Enhanced hexavalent chromium removal performance and stabilization by magnetic iron nanoparticles assisted biochar in aqueous solution: Mechanisms and application potential. Chemosphere 207, 50–59.